

# SERF 原子自旋惯性测量耦合系综响应模型研究

徐子童<sup>1,2</sup>, 魏凯<sup>2,3\*</sup>, 翟跃阳<sup>2,3</sup>, 全伟<sup>2,3</sup>, 房建成<sup>2,3</sup>

<sup>1</sup> 北京航空航天大学仪器科学与光电工程学院, 北京 100191;

<sup>2</sup> 杭州极弱磁场重大科技基础设施研究院, 浙江 杭州 310051;

<sup>3</sup> 北京航空航天大学大科学装置研究院, 北京 100191

**摘要** 无自旋交换弛豫(SERF)原子自旋惯性测量装置在前沿基础物理探索以及惯性导航领域具有广泛应用前景。建立了 SERF 原子自旋惯性测量装置的耦合系综动力学响应模型, 通过仿真和实验量化分析了耦合系综动力学响应的影响因素, 厘清了偏置磁场、耦合自旋系综极化率和弛豫率等因素对准静态响应信号的影响。发现在强耦合点与自补偿点处, 动态响应速度存在 75 倍的显著差异。进一步分析了偏置磁场、极化率和弛豫率对不同原子组合的惯性测量装置响应系数的影响。发现在自补偿点处存在最优极化率, 使惯性测量装置的角速度响应系数最高, 此最优点与原子种类和电子自旋弛豫率相关, 可以通过降低电子自旋弛豫率将角速度响应系数提升近 1 倍。明确了通过优化电子自旋极化率和抑制电子自旋弛豫率可以进一步提升 SERF 原子自旋惯性测量灵敏度和动态性能, 有望拓展其在惯性导航和基础物理探索中的应用。

**关键词** 测量; 无自旋交换弛豫; 惯性测量装置; 原子自旋耦合系综; 动力学响应模型; 自补偿

中图分类号 O562 文献标志码 A

DOI: 10.3788/CJL202249.1904001

## 1 引言

随着量子精密测量技术的发展, 基于无自旋交换弛豫(SERF)效应<sup>[1-2]</sup>的原子磁强计<sup>[3-5]</sup>和惯性测量装置在国内外成为了研究热点。SERF 原子自旋惯性测量装置目前已被广泛应用于前沿基础物理探索<sup>[6]</sup>中, 包括第五种力测量<sup>[7-9]</sup>、轴子和类轴子(ALP)的暗物质探测<sup>[10-11]</sup>以及电荷共轭、宇称反转与时间反演(CPT)和洛伦兹对称性破缺验证<sup>[12-13]</sup>, 创造了多项指标纪录。超高灵敏惯性测量装置支撑研制的原子陀螺仪在惯性导航领域具有国际公认的发展潜力<sup>[14-16]</sup>。除此之外, SERF 惯性测量装置中强耦合自旋系综的自旋操纵和检测可以应用于量子信息领域。碱金属电子可以作为光子和惰性气体核自旋之间的媒介, 应用于长寿命光量子存储器<sup>[17-18]</sup>, 也可以利用耦合系综的长相干时间实现多个气室之间长寿命的自旋纠缠。

SERF 惯性测量系统可以分为两部分: 一部分是 SERF 原子磁强计, 另一部分是与碱金属原子相互作用的核自旋系综。为了量化输入对输出信号的影响, 普林斯顿大学团队首次分析了基于 K-<sup>3</sup>He 的 SERF 惯性测量装置的响应模型, 研究了电子自旋-核自旋耦合特性<sup>[19-20]</sup>。北京航空航天大学团队建立了 Cs-<sup>129</sup>Xe 原子陀螺仪的响应模型, 分析了零偏稳定性的影响因

素<sup>[21]</sup>; 然后建立了基于 K-Rb-<sup>21</sup>Ne 混合抽运的响应模型, 分析了考虑电子等效磁场时的耦合系综特性<sup>[22]</sup>, 此项研究弥补了对电子等效磁场的考虑, 但是没有具体分析 K-Rb 原子之间的耦合关系; 之后建立混合原子动力学模型, 进行了 K-Rb-<sup>21</sup>Ne 混合抽运的噪声分析<sup>[23]</sup>。以上研究完善了 K-<sup>3</sup>He 到 K-Rb-<sup>21</sup>Ne 混合抽运的响应模型, 但并未考虑两种原子组合之间的对比, 而且对于耦合系综响应的影响因素的分析并不全面。

本文建立了惯性测量装置的耦合系综动力学响应模型, 考虑到 K-Rb-<sup>21</sup>Ne 和 K-Rb-<sup>3</sup>He 不同的电子等效磁场, 基于这两种原子组合对响应模型的影响因素进行了量化分析。研究了偏置磁场对动态响应速度的影响。进一步建立了完整的准静态响应模型, 分析了电子自旋极化率和弛豫率对准静态响应系数的影响。本研究对惯性测量装置动态性能的改善和灵敏度的提升具有重要意义, 有望推进惯性导航和前沿基础物理探索领域的发展。

## 2 基本原理

SERF 惯性测量装置利用抽运光实现电子自旋和核自旋极化, 利用检测光实现旋光角检测, 其原理如图 1 所示。首先利用激光抽运极化碱金属电子自旋,

收稿日期: 2022-05-23; 修回日期: 2022-07-10; 录用日期: 2022-07-13

基金项目: 国家自然科学基金杰出青年基金(61925301)、中国博士后科学基金(2021M700345)

通信作者: \*weikai@buaa.edu.cn

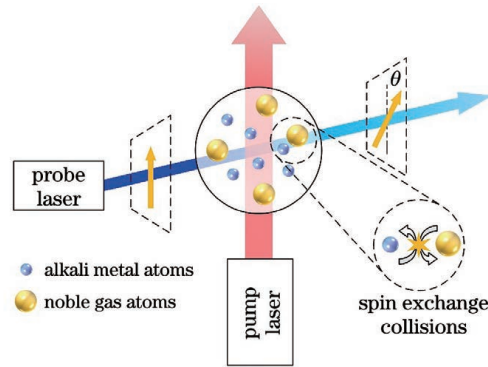


图1 抽运与检测原理示意图

Fig. 1 Schematic diagram of pump and detection principle

通过碱金属和惰性气体原子之间的自旋交换碰撞使惰性气体核自旋实现超极化。核自旋敏感惯性转动信号而发生自旋进动,再利用碱金属电子自旋测量惰性气体核自旋磁矩的进动信号,原子自旋进动信息最终可反映为对检测光线偏振面旋转角 $\theta$ 的检测,从而实现惯性测量。

电子自旋和核自旋之间的自旋交换碰撞作用可以用 Bloch 方程描述<sup>[24-26]</sup> :

$$\left\{ \begin{array}{l} \frac{\partial \mathbf{P}^e}{\partial t} = \frac{\gamma^e}{Q} (\mathbf{B} + \mathbf{L} + \mathbf{B}^n + \mathbf{b}^e) \times \mathbf{P}^e - \\ \quad \boldsymbol{\Omega} \times \mathbf{P}^e + \frac{R_p \mathbf{s}_p + R_m \mathbf{s}_m + R_{se}^{en} \mathbf{P}^n}{Q} - \\ \quad \frac{\{R_1^e, R_2^e, R_2^n\}}{Q} \mathbf{P}^e \\ \frac{\partial \mathbf{P}^n}{\partial t} = \gamma^n (\mathbf{B} + \mathbf{B}^e + \mathbf{b}^n) \times \mathbf{P}^n - \boldsymbol{\Omega} \times \mathbf{P}^n + \\ \quad R_{se}^{ne} \mathbf{P}^e - \{R_1^n, R_2^n, R_2^n\} \mathbf{P}^n \end{array} \right. , \quad (1)$$

式中:上标 e 和 n 分别表示电子自旋和核自旋;  $\mathbf{P}$  代表极化率;  $\gamma$  为旋磁比; Q 为减慢因子,与电子自旋极化率相关;  $\mathbf{B}$  为环境磁场;  $\mathbf{B}^n$  和  $\mathbf{B}^e$  分别为碱金属电子自旋感受到的惰性气体核自旋磁场和惰性气体核自旋

感受到的碱金属电子自旋磁场;  $\mathbf{L}$  是光频移;  $\boldsymbol{\Omega}$  为转动角速度;  $R_p$  为光抽运率,其光子自旋为  $\mathbf{s}_p$ ;  $R_m$  为检测光抽运率,其光子自旋为  $\mathbf{s}_m$ ;  $R_{se}^{en}$  和  $R_{se}^{ne}$  分别为核自旋抽运率和电子自旋抽运率;  $R_1^e (R_2^e)$  和  $R_1^n (R_2^n)$  为分别碱金属电子自旋纵向(总)弛豫率和惰性气体核自旋纵向(总)弛豫率。总弛豫率中包括自旋交换弛豫率  $R_{rel}^{se}$ ,此弛豫率受到偏置磁场和电子自旋极化率的显著影响,在 K-Rb-<sup>21</sup>Ne 系统中不可忽略,其表达式为

$$R_{rel}^{se} = \frac{\omega_e^2}{R_{se}} \frac{Q^2 - (2I+1)^2}{2}, \quad (2)$$

式中: $\omega_e$  为电子自旋的进动频率; $R_{se}$  为自旋交换率; $I$  为核自旋。

本文考虑自旋交换弛豫率  $R_{rel}^{se}$ ,完善了耦合系综动力学模型,进一步分析了各种影响因素对动态响应的影响。当输入的横向(正交于抽运光的方向)信号较小时,对自旋系综极化率的纵向(抽运光的方向,定义为 z 轴)分量的影响可以忽略,因而碱金属电子和惰性气体核自旋的纵向极化率近似保持不变,即  $\partial P_z^e / \partial t = 0$  和  $\partial P_z^n / \partial t = 0$ 。进而可以消除纵向极化率与横向极化率之间的耦合,将 Bloch 方程组简化,得到电子的横向极化率为<sup>[27]</sup>

$$P_{\perp}^e = K_{\perp}^e e^{\lambda_{\perp}^e t} + K_{\perp}^n e^{\lambda_{\perp}^n t} + P_{\perp-\text{steady}}^e. \quad (3)$$

式(3)右边三项分别表示电子自旋和核自旋两个系综的振荡衰减过程以及稳态信号。其中,  $P_{\perp}^e = P_x^e + iP_y^e$  代表电子横向极化率,  $K_{\perp}^e = K_{er} + iK_{ei}$  和  $K_{\perp}^n = K_{nr} + iK_{ni}$  分别代表电子和核子的瞬态响应系数,  $\lambda_{\perp}^e = \lambda_{er} + i\lambda_{ei}$  和  $\lambda_{\perp}^n = \lambda_{nr} + i\lambda_{ni}$  分别表示电子和核子的衰减振荡,  $P_{\perp-\text{steady}}^e = P_{x-\text{steady}}^e + iP_{y-\text{steady}}^e$  描述了稳态响应强度。

由于 x 和 y 轴具有对称性,而本文的检测光沿 x 轴,只研究 x 方向的输出,将式(3)展开可以得到:

$$P_x^e = e^{\lambda_{er} t} P_{er} \cos(\lambda_{ei} t) + e^{\lambda_{nr} t} P_{nr} \cos(\lambda_{ni} t) - e^{\lambda_{er} t} P_{ei} \sin(\lambda_{ei} t) - e^{\lambda_{nr} t} P_{ni} \sin(\lambda_{ni} t) + P_{x-\text{steady}}^e. \quad (4)$$

$\lambda_{er}$  和  $\lambda_{nr}$  分别表示电子自旋和核自旋的衰减阻尼,  $\lambda_{ei}$  和  $\lambda_{ni}$  分别为电子自旋和核自旋的特征频率,它们描述了电子自旋和核自旋耦合系综的动态性能。

根据式(1)进行求解,可以得到:

$$\left\{ \begin{array}{l} \lambda_{nr} = -\frac{R_2^n + \frac{R_2^e}{Q}}{2} + \frac{\sqrt{\sqrt{c_1^2 + c_2^2} + c_1}}{2\sqrt{2}} \\ \lambda_{ni} = \frac{\omega_n + \omega_e}{2} + \frac{\text{sgn}(c_2) \sqrt{\sqrt{c_1^2 + c_2^2} - c_1}}{2\sqrt{2}} \\ \lambda_{er} = -\frac{R_2^n + \frac{R_2^e}{Q}}{2} - \frac{\sqrt{\sqrt{c_1^2 + c_2^2} + c_1}}{2\sqrt{2}} \\ \lambda_{ei} = \frac{\omega_n + \omega_e}{2} - \frac{\text{sgn}(c_2) \sqrt{\sqrt{c_1^2 + c_2^2} - c_1}}{2\sqrt{2}} \end{array} \right. , \quad (5)$$

$$\begin{cases} c_1 = (R_2^e/Q - R_2^n)^2 - (\omega_e - \omega_n)^2 + 4R_{se}^{ne}R_{se}^n/Q - 4\omega_{ne}\omega_{en}, \\ c_2 = -2(R_2^e/Q - R_2^n)(\omega_e - \omega_n) - 4(R_{se}^{ne}\omega_{ne}/Q + R_{se}^n\omega_{en}), \end{cases} \quad (6)$$

式中: $\omega_e = \gamma^e(B_z + B_z^n)/Q$  和  $\omega_n = \gamma^n(B_z + B_z^e)$  分别表示电子自旋和核自旋的进动频率; $\omega_{en} = \gamma^e\lambda M_z P_z^e/Q$ ,  $\omega_{ne} = \gamma^n\lambda M_z^e P_z^n$ 。当两个自旋系综的进动频率相等时,即  $B_z = \frac{\gamma^n Q B_z^e - \gamma^e B_z^n}{\gamma^e - \gamma^n Q}$  时,核子的衰减阻尼通过与电子耦合而增大,我们将此点定义为强耦合点。

SERF 惯性测量系统中,主要的输入信号包括转动信号  $\Omega$ 、磁场信号  $\mathbf{B}$ 、光频移信号  $\mathbf{L}$  以及可能存在的异常场信号  $\mathbf{b}$ 。稳态信号可以表示为

$$P_x^e \approx \frac{\gamma^e P_z^e R_2^e}{[\gamma^e(\delta B_z + L_z - \Omega_z/\gamma^n)]^2 + (R_2^e)^2} \cdot \left\{ b_y^e + L_y - \frac{\delta B_z}{B_z^n} B_y - \left( \frac{\gamma^e - Q\gamma^n}{\gamma^e\gamma^n} + \frac{\delta B_z}{\gamma^n B_z^n} \right) \Omega_y - \left( 1 + \frac{\delta B_z}{B_z^n} \right) b_y^n + \frac{\gamma^e}{R_2^e} (\delta B_z + L_z - \Omega_z/\gamma^n) \times \left[ b_x^e + L_x - \frac{\delta B_z}{B_z^n} B_x - \left( \frac{\gamma^e - Q\gamma^n}{\gamma^e\gamma^n} + \frac{\delta B_z}{\gamma^n B_z^n} \right) \Omega_x - \left( 1 + \frac{\delta B_z}{B_z^n} \right) b_x^n \right] \right\}, \quad (7)$$

式中: $\delta B_z = B_z - (-B_z^e - B_z^n + \Omega_z/\gamma^n)$ 。

可以看出,如果光频移接近于零,且  $\Omega_z$  可以忽略,当  $B_z = -B_z^e - B_z^n$  时,  $P_x^e$  只响应异常作用场  $b_y^e$ 、 $b_y^n$  和角速度  $\Omega_y$  的输入,也就是说,当偏置磁场恰好抵消电子和核子等效磁场之和时,  $P_x^e$  对横向磁场输入不敏感。这种现象被称为核自旋自补偿效应<sup>[14]</sup>,是 SERF 惯性测量装置能够抑制外界低频磁噪声的关键。此时的偏置磁场被称为自补偿点。一般情况下,惯性测量装置工作于此点。

系统中的噪声信号主要包括磁场信号  $\mathbf{B}$ 、转动信号  $\Omega$ 、光频移信号  $\mathbf{L}$  以及抽运光横向投影分量项  $R_p$  和检测光圆偏振分量项  $R_m$ 。式(7)所建立的响应信号模型中忽略了交叉耦合项、高阶项以及  $R_{se}^{ne}$ 、 $R_{se}^n$ 、 $R_2^n$  的影响,而在 SERF 惯性测量系统的实际测量中,误差

信号相关的交叉耦合项和高阶项会引入系统噪声,与转动信号相关的交叉耦合项和高阶项会导致刻度系数标定误差。另外,惰性气体核自旋的实际横向弛豫率比理论计算值大 2~3 个数量级,各响应信号中与其相关的项会引入测量误差。对每种噪声信号建立完整的响应模型,并进行具体的量级分析。纵向光频移和核自旋横向弛豫率会导致  $\Omega_x$  和  $\Omega_y$  的耦合,需要对纵向光频移进行消除;核自旋横向弛豫率还会导致自补偿抑制磁场  $B_x$  的能力较差,使  $B_x$  噪声成为系统中主要的噪声源; $R_p$  和  $R_m$  是一阶噪声项,因此需要减小抽运光和检测光之间的非正交角和检测光圆偏振分量。

从式(7)可以得到稳态响应对不同输入的响应系数:

$$\left\{ \begin{array}{l} K_{B_y} = \frac{-\gamma^e P_z^e R_2^e}{[\gamma^e(\delta B_z + L_z - \Omega_z/\gamma^n)]^2 + (R_2^e)^2} \frac{\delta B_z}{B_z^n} \\ K_{b_y^e} = \frac{\gamma^e P_z^e R_2^e}{[\gamma^e(\delta B_z + L_z - \Omega_z/\gamma^n)]^2 + (R_2^e)^2} \\ K_{b_y^n} = \frac{-\gamma^e P_z^e R_2^e}{[\gamma^e(\delta B_z + L_z - \Omega_z/\gamma^n)]^2 + (R_2^e)^2} \left( 1 + \frac{\delta B_z}{B_z^n} \right) \\ K_{\Omega_y} = \frac{-\gamma^e P_z^e R_2^e}{[\gamma^e(\delta B_z + L_z - \Omega_z/\gamma^n)]^2 + (R_2^e)^2} \left( \frac{\gamma^e - Q\gamma^n}{\gamma^e\gamma^n} + \frac{\delta B_z}{\gamma^n B_z^n} \right) \end{array} \right. . \quad (8)$$

从式(8)可以看出,影响稳态响应信号强度的主要因素为  $\delta B_z$ 、 $P_z^e$  以及  $R_2^e$ 。对于 K-Rb-<sup>3</sup>He 系统来说,电子等效磁场远小于核子等效磁场,因此自补偿点和强耦合点几乎相等。然而,对于 K-Rb-<sup>21</sup>Ne 系统来说,电子等效磁场无法忽略,自补偿点和强耦合点相距 100 nT 左右<sup>[22]</sup>。同时,这也导致电子无法处于理想的 SERF 态,自旋交换弛豫率也无法忽略,因此本文分别进行两种原子组合的讨论。

### 3 实验

实验装置如图 2 所示。所用直径 12 mm 的 K-

Rb-<sup>21</sup>Ne 气室处于装置中心,其中充有少量 K 和自然丰度的 Rb,约 7200 Pa 的 N<sub>2</sub>,以及约  $3.33 \times 10^5$  Pa 的氖气(<sup>21</sup>Ne 的丰度 70%)。利用光频移法原位测量 K 和 Rb 的密度比,在 200 °C 时约为 1/187<sup>[28]</sup>。气室安装在氮化硼陶瓷烤箱中,在烤箱的外壁粘贴电加热膜,该加热膜采用双层对绕结构,另外利用高频交流电供电,从而减小加热电流引入的低频磁噪声。为提升气室温度稳定性,利用铂电阻测量气室壁温度,进行 PID 闭环控制。为了减小气室加热时与外界温差导致的空气对流,将烤箱与气室整体置于聚醚醚酮(PEEK)材质的真空腔中,真空间度可以降至 700~800 Pa。最外

层利用五层坡莫合金进行磁屏蔽。坡莫合金虽然具有较高的磁屏蔽系数,但是电阻率低,会产生涡流损耗噪声,因此在坡莫合金磁屏蔽桶内增加一层电阻率更高的锰锌铁氧体,降低Johnson电流噪声。三维磁场线圈在原子气室区域产生均匀的三维磁场,实现磁屏蔽桶内的剩磁补偿。抽运光为圆偏振光,波长为770.108 nm,检测光为线偏振光,波长为795.500 nm,均采用优立光太激光器,光斑直径分别为13.5 mm和2.5 mm。利用光弹性调制器(PEM, II/FS50LR, Hinds Instruments)将检测信号调制到千赫兹量级的高频段<sup>[29-30]</sup>,然后通过锁相放大器(HF2LI, Zurich Instrument)实现旋光信号的解调,从而实现低频检测噪声的抑制。

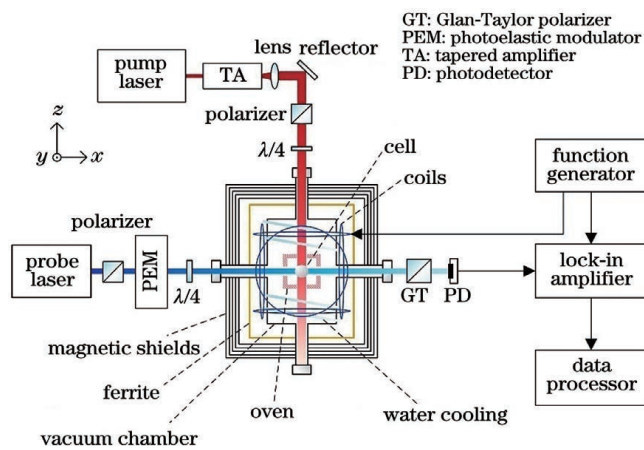


图2 SERF惯性测量实验装置图

Fig. 2 Experimental setup of SERF comagnetometer

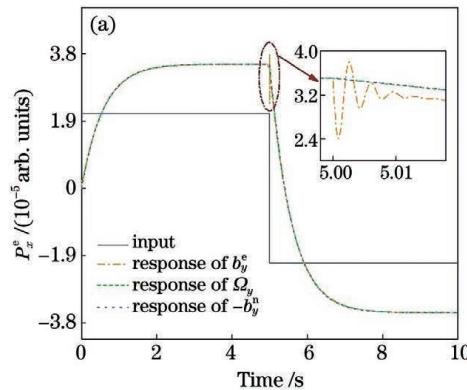


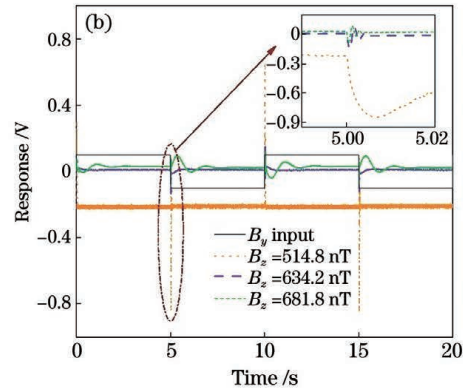
图3 方波输入响应结果(插图为将主图特定部分放大的图像)。(a)异常场和角速度响应;

Fig. 3 Response results of square wave input (inset is enlarged image of certain part of main image). (a) Responses to anomalous fields and angular velocity; (b) responses to magnetic field under different bias magnetic fields

在电子自旋极化率为0.5时,分别仿真了K-Rb-<sup>21</sup>Ne和K-Rb-<sup>3</sup>He系统中偏置磁场对 $K_{B_y}$ 、 $K_{b_y^e}$ 、 $K_{b_y^n}$ 和 $K_{\Omega_y}$ 的影响,结果如图4所示。图4(a)~图4(d)是K-Rb-<sup>21</sup>Ne系统中的仿真结果,图4(e)~图4(h)是K-Rb-<sup>3</sup>He系统中的仿真结果。其中 $K_{B_y}$ 在 $\delta B_z = 0$ 即处于自补偿点时为零,说明对磁场无响应。对异常场和角速度的响应系数均在补偿点处达到

## 4 结果与讨论

首先对建立的动态响应模型和稳态响应模型的正确性进行了仿真和实验验证。对K-Rb-<sup>21</sup>Ne系统中补偿点处的异常场和角速度输入进行了仿真,其中K-Rb密度比为1/152,温度190 ℃,电子自旋极化率为0.5, $b_y^e$ 、 $b_y^n$ 、 $\Omega_y/\gamma^n$ 均为1 pT(为了清楚地表现方波输入,对方波信号进行了幅值放大),得到的结果如图3(a)所示。从图3(a)主图中可以看出,惯性测量系统对角速度和异常场的作用较为敏感,且响应过程基本重合,稳态值几乎相等,与式(7)完全相符。插图是将方波输入下降沿处的瞬态响应进行放大的结果,仅在 $b_y^e$ 输入时,瞬态响应中会包含电子的快速衰减振荡过程,因为电子并不直接敏感角速度和核自旋耦合异常场,而是通过敏感核自旋的进动来实现测量。在K-Rb-<sup>21</sup>Ne惯性测量装置中测量了不同偏置磁场下的磁场输入响应,如图3(b)所示。在光功率为493.8 mW/cm<sup>2</sup>时,输入幅值为0.24 nT的方波磁场,测量了自补偿点(634.2 nT)、强耦合点(514.8 nT)以及另一普通工作点(681.8 nT)处的响应。图中划线的稳态值接近于零,而且方波上下沿对应的稳态输出信号之差也几乎为零,达到稳态所需时间约3.7 s,结合式(7),说明此处为自补偿点。图中点线的衰减振荡过程最短暂,约为50 ms,比自补偿点时快约75倍,说明此时动态性能最好。此外,从图3(b)的插图中可以看出,此时的电子振荡过程与核子融为一体,说明两者处于强耦合状态,此处为强耦合点。在另一个普通的工作点[图3(b)中短划线],既无法抑制磁场输入,达到稳态所需时间也很长。



最大值,远离补偿点处逐渐趋近于零。因此在自补偿点工作时,SERF惯性测量装置可以实现对异常场和角速度的超高灵敏测量,从而有潜力进行前沿物理探索和惯性导航。比较两个不同的核子系统,可以看出K-Rb-<sup>21</sup>Ne对角速度的响应系数比K-Rb-<sup>3</sup>He高近5倍,因为<sup>21</sup>Ne核子旋磁比仅为<sup>3</sup>He核子旋磁比的1/10左右,同时<sup>21</sup>Ne系统中的电子总弛豫率比<sup>3</sup>He系

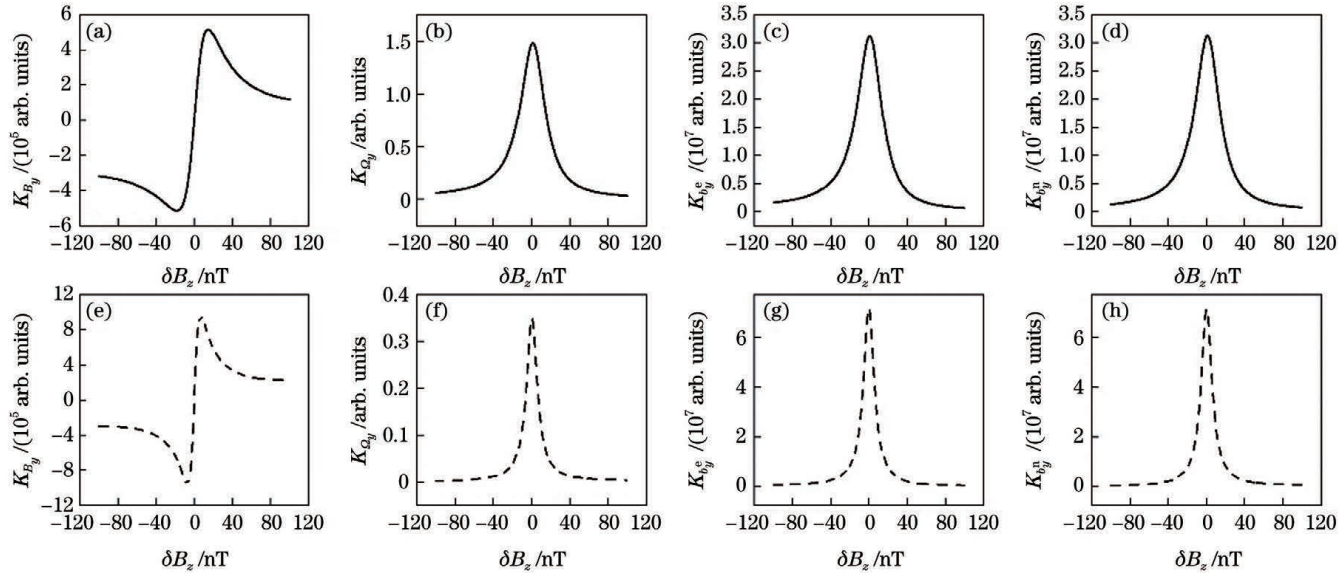
图4 响应系数与偏置磁场的关系。(a)~(d)K-Rb-<sup>21</sup>Ne系统中的系数;(e)~(h)K-Rb-<sup>3</sup>He系统中的系数

Fig. 4 Relationship between response coefficients and bias magnetic field. (a)–(d) Coefficients in K-Rb-<sup>21</sup>Ne system; (e)–(h) coefficients in K-Rb-<sup>3</sup>He system

统中高2~3倍。

为了进一步研究角速度响应强度的影响因素,分析了在自补偿点处的 $K_{\Omega_y}$ 随极化率和弛豫率的变化情况,仿真结果如图5所示。在K-Rb-<sup>3</sup>He系统中, $K_{\Omega_y}$ 随极化率先增后减,在极化率为0.5时达到最大值,并且最大值随着电子自旋弛豫率的减小而增大。当电子自旋弛豫率从800 rad/s降至400 rad/s时,响应系数 $K_{\Omega_y}$ 由0.26提高至0.51,提高了近一倍。在

K-Rb-<sup>21</sup>Ne系统中, $K_{\Omega_y}$ 同样随极化率增大而先增后减,但在极化率处于0.3~0.7时, $K_{\Omega_y}$ 增长较为缓慢。随着电子自旋弛豫率的减小,最大的响应系数从1.48提高至2.31,同时响应系数最大值所对应的极化率逐渐提高。对比两种原子组合,尽管K-Rb-<sup>21</sup>Ne系统中并非理想SERF态,但它对于角速度的响应依然强于K-Rb-<sup>3</sup>He系统。除此之外,降低电子自旋弛豫率可以有效增大响应系数。

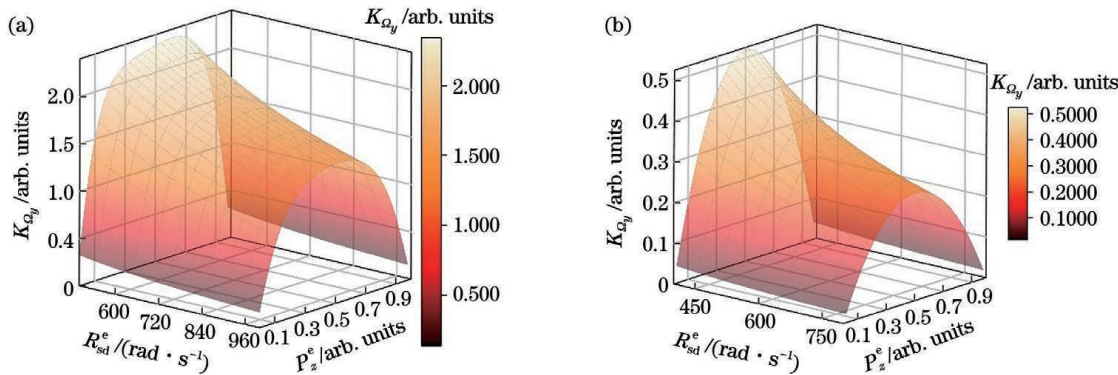


图5 自补偿点处响应系数与电子自旋极化率和弛豫率的关系。(a)K-Rb-<sup>21</sup>Ne系统中的系数;(b)K-Rb-<sup>3</sup>He系统中的系数  
Fig. 5 Dependence of response coefficients on electronic spin polarization and relaxation rate at compensation point. (a) Coefficients in K-Rb-<sup>21</sup>Ne system; (b) coefficients in K-Rb-<sup>3</sup>He system

## 5 结 论

本文建立了完整的SERF惯性测量系统的耦合系综动力学响应模型。对K-Rb-<sup>3</sup>He系统进行仿真,利用K-Rb-<sup>21</sup>Ne装置进行实验,验证了所建立模型的正确性。动态响应速度受到偏置磁场的影响十分显著,基于本文的实验温度和光功率等实验条件,在工作于强耦合点处时响应速度比工作于自补偿点时的响应速度快75倍。通过仿真量化分析了稳态响

应强度的影响因素,稳态响应主要受到电子自旋极化率和电子自旋弛豫率的影响,存在最优极化率,使角速度响应系数达到最大。同时,弛豫率的减小可以将K-Rb-<sup>3</sup>He系统的角速度响应系数由0.26提高至0.51,将K-Rb-<sup>21</sup>Ne系统的角速度响应系数由1.48提高至2.31。因此,通过降低电子自旋弛豫率可以实现响应系数的提高,从而提高惯性测量灵敏度,为前沿物理探索和惯性导航领域的发展提供良好基础。

## 参考文献

- [1] Happer W, Tang H. Spin-exchange shift and narrowing of magnetic resonance lines in optically pumped alkali vapors [J]. Physical Review Letters, 1973, 31(5): 273-276.
- [2] Happer W, Tam A C. Effect of rapid spin exchange on the magnetic-resonance spectrum of alkali vapors [J]. Physical Review A, 1977, 16(5): 1877-1891.
- [3] 陈伯韬, 江敏, 季云兰, 等. 用于零场核磁共振探测的无自旋交换弛豫原子磁力仪[J]. 中国激光, 2017, 44(10): 1004001.
- Chen B T, Jiang M, Ji Y L, et al. Spin-exchange relaxation free atomic magnetometer for zero-field nuclear magnetic resonance detection[J]. Chinese Journal of Lasers, 2017, 44(10): 1004001.
- [4] 吴梓楠, 赵正钦, 温钟平, 等. 高灵敏度微型光学原子磁力仪研究进展[J]. 激光与光电子学进展, 2020, 57(23): 230002.
- Wu Z N, Zhao Z Q, Wen Z P, et al. Research progress on high sensitivity and miniature optical-atomic magnetometer[J]. Laser & Optoelectronics Progress, 2020, 57(23): 230002.
- [5] 王宇, 赵惟玉, 康翔宇, 等. SERF 原子磁强计最新进展及应用综述[J]. 光学仪器, 2021, 43(6): 77-86.
- Wang Y, Zhao W Y, Kang X Y, et al. The latest development and application of SERF atomic magnetometer: a review [J]. Optical Instruments, 2021, 43(6): 77-86.
- [6] Safranova M S, Budker D, DeMille D, et al. Search for new physics with atoms and molecules [J]. Reviews of Modern Physics, 2018, 90(2): 025008.
- [7] Ji W, Chen Y, Fu C B, et al. New experimental limits on exotic spin-spin-velocity-dependent interactions by using SmCo<sub>5</sub> spin sources[J]. Physical Review Letters, 2018, 121(26): 261803.
- [8] Almasi A, Lee J Y, Winarto H, et al. New limits on anomalous spin-spin interactions [J]. Physical Review Letters, 2020, 125(20): 201802.
- [9] Wang Z G, Peng X, Zhang R, et al. Single-species atomic comagnetometer based on <sup>87</sup>Rb atoms [J]. Physical Review Letters, 2020, 124(19): 193002.
- [10] Graham P W, Kaplan D E, Mardon J, et al. Spin precession experiments for light axionic dark matter [J]. Physical Review D, 2018, 97(5): 055006.
- [11] Terrano W A, Romalis M V. Comagnetometer probes of dark matter and new physics [J]. Quantum Science and Technology, 2022, 7(1): 014001.
- [12] Brown J M, Smullin S J, Kornack T W, et al. New limit on Lorentz- and CPT-violating neutron spin interactions[J]. Physical Review Letters, 2010, 105(15): 151604.
- [13] Allmendinger F, Heil W, Karpuk S, et al. New limit on Lorentz-invariance- and CPT-violating neutron spin interactions using a free-spin-precession <sup>3</sup>He-<sup>129</sup>Xe comagnetometer[J]. Physical Review Letters, 2014, 112(11): 110801.
- [14] Kornack T W, Ghosh R K, Romalis M V. Nuclear spin gyroscope based on an atomic comagnetometer [J]. Physical Review Letters, 2005, 95(23): 230801.
- [15] Zhang C, Yuan H, Tang Z, et al. Inertial rotation measurement with atomic spins: from angular momentum conservation to quantum phase theory [J]. Applied Physics Reviews, 2016, 3(4): 041305.
- [16] Li R J, Fan W F, Jiang L W, et al. Rotation sensing using a K-Rb-<sup>21</sup>Ne comagnetometer[J]. Physical Review A, 2016, 94(3): 032109.
- [17] Katz O, Shaham R, Firstenberg O. Coupling light to a nuclear spin gas with a two-photon linewidth of five millihertz [J]. Science Advances, 2021, 7(14): abe9164.
- [18] Katz O, Shaham R, Polzik E S, et al. Long-lived entanglement generation of nuclear spins using coherent light [J]. Physical Review Letters, 2020, 124(4): 043602.
- [19] Kornack T W, Romalis M V. Dynamics of two overlapping spin ensembles interacting by spin exchange [J]. Physical Review Letters, 2002, 89(25): 253002.
- [20] 秦杰. 基于<sup>129</sup>Xe-Cs 的 SERF 原子自旋陀螺仪原理实验研究[D]. 北京:北京航空航天大学, 2012: 28-30.
- Qin J. Experimental development of SERF atomic spin gyroscope based on <sup>129</sup>Xe-Cs[D]. Beijing: Beihang University, 2012: 28-30.
- [21] 万双爱. SERF 原子自旋陀螺仪的误差分析及其抑制方法实验研究[D]. 北京: 北京航空航天大学, 2014: 29-33.
- Wan S A. Error analysis of SERF atomic spin gyroscope and experimental study on its suppression method [D]. Beijing: Beihang University, 2014: 29-33.
- [22] Fang J C, Chen Y, Lu Y, et al. Dynamics of Rb and <sup>21</sup>Ne spin ensembles interacting by spin exchange with a high Rb magnetic field[J]. Journal of Physics B: Atomic Molecular and Optical Physics, 2016, 49(13): 135002.
- [23] 魏凯. SERF 惯性测量中耦合系综自旋交换弛豫与自补偿特性研究[D]. 北京:北京航空航天大学, 2020: 47-55.
- Wei K. Study on spin-exchange relaxation and self-compensation of coupled spin ensembles in SERF comagnetometer [D]. Beijing: Beihang University, 2020: 47-55.
- [24] Chen Y, Quan W, Zou S, et al. Spin exchange broadening of magnetic resonance lines in a high-sensitivity rotating K-Rb-<sup>21</sup>Ne co-magnetometer[J]. Scientific Reports, 2016, 6: 36547.
- [25] Wei K, Zhao T, Fang X J, et al. Simultaneous determination of the spin polarizations of noble-gas and alkali-metal atoms based on the dynamics of the spin ensembles [J]. Physical Review Applied, 2020, 13(4): 044027.
- [26] Xu Z T, Wei K, Zhao T, et al. Fast dynamic frequency response-based multiparameter measurement in spin-exchange relaxation-free comagnetometers [J]. IEEE Transactions on Instrumentation and Measurement, 2021, 70: 7007110.
- [27] Quan W, Wei K, Zhao T, et al. Synchronous measurement of inertial rotation and magnetic field using a K-Rb-<sup>21</sup>Ne comagnetometer [J]. Physical Review A, 2019, 100 (1): 012118.
- [28] Wei K, Zhao T, Fang X J, et al. *In-situ* measurement of the density ratio of K-Rb hybrid vapor cell using spin-exchange collision mixing of the K and Rb light shifts[J]. Optics Express, 2019, 27(11): 16169-16183.
- [29] Ho H P, Law W C, Wu S Y, et al. Phase-sensitive surface plasmon resonance biosensor using the photoelastic modulation technique[J]. Sensors and Actuators B: Chemical, 2006, 114(1): 80-84.
- [30] Smiciklas M, Vernaza A, Romalis M V. Test of Lorentz invariance at the Amundsen-Scott South Pole Station[C]//APS Division of Atomic, Molecular and Optical Physics, June 3-7, 2013, Quebec City, Canada. New York: APS, Bulletin of the American Physical Society, 2013, 58(6): Q1.7.

# Research of Coupled Ensemble Response Model in SERF Comagnetometers

Xu Zitong<sup>1,2</sup>, Wei Kai<sup>1,2\*</sup>, Zhai Yueyang<sup>2,3</sup>, Quan Wei<sup>2,3</sup>, Fang Jiancheng<sup>2,3</sup>

<sup>1</sup> School of Instrumentation and Optoelectronic Engineering, Beihang University, Beijing 100191, China;

<sup>2</sup> Institute of Extremely-Weak-Magnetic-Field Massive Scientific Instrumentation Facility, Hangzhou 310051, Zhejiang, China;

<sup>3</sup> Institute of Large-Scale Scientific Facility, Beihang University, Beijing 100191, China

## Abstract

**Objective** Spin-exchange relaxation-free (SERF) comagnetometers have been widely applied in fundamental physics exploration, including the fifth force measurement, dark matter detection (axion and axion-like particles) and CPT (charge conjugation, parity inversion, time reversal) and Lorentz symmetry violations. Besides, it has an internationally recognized development potential in inertial navigation. SERF comagnetometers contains alkali metal electronic spin ensemble and noble gas nuclear spin ensemble. The study of the responses to external excitations inevitably involves the coupling of two ensembles. A general response model for K-<sup>3</sup>He comagnetometer has been introduced to characterize the dynamics of the hybrid pumping K-Rb-<sup>21</sup>Ne comagnetometer. However, there are significant differences between the two kinds of spin ensembles combinations. The unexplored comparison of dynamics between the two spin ensembles combinations would present fruitful discoveries. In this paper, we establish a complete model for K-Rb-<sup>21</sup>Ne comagnetometer and compare the responses of K-<sup>3</sup>He and K-Rb-<sup>21</sup>Ne comagnetometers. The influencing factors of the response rate and the amplitude are quantified. This research sheds light on the study of the difference between different spin ensembles combinations for the improvement of the dynamic performance and sensitivity of comagnetometers, and is expected to promote the development of inertial navigation and fundamental physics exploration.

**Methods** In this paper, transient and steady-state response models are established from the Bloch equations that describe the coupling of electronic and nuclear spins. In the K-Rb-<sup>21</sup>Ne comagnetometer, the electronic effective magnetic field cannot be ignored, so the spin exchange relaxation rate is considered in the model. Based on the established model, the influence of various influencing factors on the dynamic response is analyzed. For the transient response, the main influencing factor is the bias magnetic field. The dynamic responses to the magnetic field, angular velocity and anomalous field at the compensation point and the strong coupling point are compared through experiments and simulations. For the steady-state response, the relationship between response coefficients and bias magnetic field for different input signals is simulated. In order to further study the influencing factors of the angular velocity response strength, we analyze the variation of the angular velocity response coefficient with electronic spin polarization and relaxation rate at the self-compensation point.

**Results and Discussions** The dynamic response model of coupled ensembles in the SERF comagnetometer is established, and the influencing factors of the dynamic response are quantitatively analyzed with simulation and experiments. The effects of bias magnetic field, coupled spin ensemble polarization, electronic spin relaxation rate and other factors on the steady response signal are clarified. We find that there is a significant difference of 75 times in the dynamic response rate between the strong coupling point and the self-compensation point (Fig. 3). Besides, the response strengths to different input signals are simulated under various bias magnetic fields. At the self-compensation point, the responses of comagnetometer to the anomalous field and inertial rotation are maximized, while the sensitivity to the magnetic field is minimized (Fig. 4). It is further analyzed that there is an optimal polarization at the self-compensation point, which makes the angular velocity response coefficient the highest (Fig. 5). This optimal point is related to the atomic species and the electronic spin relaxation rate, at which the angular velocity response coefficient can be doubled by reducing the electronic spin relaxation rate. This paper clarifies that the sensitivity and dynamic performance of SERF comagnetometers can be further improved by optimizing the electronic spin polarization and the relaxation rate, which is expected to expand its application in inertial navigation and fundamental physics exploration.

**Conclusions** In the present study, a complete coupled ensemble dynamic response model of the SERF comagnetometer is established. The dynamics of K-Rb-<sup>3</sup>He system is studied via simulation, and the dynamics of K-Rb-<sup>21</sup>Ne system is experimentally studied to verify the correctness of the established model. The dynamic response rate is found to be significantly affected by the bias magnetic field. Based on the experimental conditions such as the experimental temperature and optical power in this paper, the response rate at the strong coupling point is 75 times faster than that at the self-compensation point. The influencing factors of the steady-state response strength are quantitatively analyzed by simulation. The steady-state response is mainly affected by the electronic spin polarization and the electronic spin

relaxation rate. There is an optimal polarization which maximizes the angular velocity response coefficient. At the same time, the decrease of the electronic spin relaxation rate can increase the angular velocity response coefficient of the K-Rb-<sup>3</sup>He system from 0.26 to 0.51, and that of the K-Rb-<sup>21</sup>Ne system from 1.48 to 2.31. Therefore, by reducing the electronic spin relaxation rate and optimizing the electronic spin polarization, the response coefficient can be improved, thereby improving the sensitivity of inertial measurement, providing a good foundation for the development of fundamental physics exploration and inertial navigation.

**Key words** measurement; spin-exchange relaxation-free; comagnetometer; coupled spin ensembles; dynamics response model; self compensation